Interaction of differently functionalized fluorescent silica nanoparticles with neural stem- and tissue-type cells

EMILIA IZAK*, KATA KENESEI, KUMARASAMY MURALI, MATTHIAS VOETZ, STEFANIE EIDEN, VICTOR F. PUNTES, ALBERT DUSCHL AND EMILIA MADARÁSZ

[*] E. Izak,
Dr. M. Voetz, Dr. S. Eiden
Bayer Technology Services GmbH
51368 Leverkusen (Germany)
E-mail: emilia.izak@bayer.com

Dr. E. Madarász, K. Kenesei, K. Murali
Institute of Experimental Medicine, Hungarian Academy of Sciences
1083 Budapest (Hungary)

Prof. V.F. Puntes
Catalan Institute of Nanotechnology (ICN)
Campus UAB, Edifici CIN2
08193 Bellaterra, Barcelona (Spain)

Prof. A. Duschl, E. Izak
Department of Molecular Biology, University of Salzburg
5020 Salzburg (Austria)

Supporting Information is available on the WWW under http://www.small-journal.com or from the author.

Keywords: Silica NP, neural cell types, toxicity, uptake, fluorescence spectrum analysis

Abstract

Engineered amorphous silica nanoparticles (SiO_2 NPs), due to simple and low cost production, are increasingly used in commercial products and produced on an industrial scale. Despite the potential benefits, there is a concern that exposure to certain types of SiO_2 NPs may lead to adverse health effects. As some NPs can cross the blood-brain barrier and may, in addition, reach the central nervous system through the nasal epithelium, this study addresses the responses of different neural tissue-type cells including neural stem cells, neurons, astrocytes and microglia cells to increasing doses of 50 nm fluorescent core/shell SiO_2 NPs with different (-NH_2, -SH and polyvinylpyrrolidone (PVP)) surface chemistry. The SiO_2 NPs are characterized using a variety of physicochemical methods.

Assays of cytotoxicity and cellular metabolism indicates that SiO_2 NPs cause cell death only at high particle doses, except PVP-coated SiO_2 NPs which do not harm cells even at very high concentrations. All SiO_2 NPs, except those coated with PVP, form large agglomerates in physiological solutions and adsorb a variety of proteins. Except PVP-NPs, all SiO_2 NPs adhere strongly to cell surfaces, but internalization differs depending on neural cell type. Neural stem cells and astrocytes internalize plain SiO_2, SiO_2-NH_2, and SiO_2-SH NPs, while neurons do not take up any NPs. The data indicates that the PVP coat, by lowering the particle-biomolecular component interactions, reduces the biological effects of SiO_2 NPs on the investigated neural cells.

Introduction

Nanoparticles (NPs) exhibit a variety of unique chemical and physical properties that have made them central components in an array of emerging technologies. Among various NPs that have found commercial application, silica NPs (SiO_2 NPs) are produced on an industrial scale, as additives to cosmetics, drugs, printer toners and foods. SiO_2 NPs are achieving applications in biotechnology and biomedicine as drug delivery systems (Slowing et al. 2008), anti-cancer

therapeutics (Hirsch et al. 2003), enzyme immobilizers and DNA transfecting agents (Vijayanathan et al. 2002; Ravi Kumar et al. 2004). Due to the simplicity of tailoring surface reactivity via surface functionalization (Walcarius and Ganesan 2006), SiO_2 NPs are also suitable subjects for basic studies on surface-dependent NP-performance. They can be conjugated with a variety of fluorophores, to produce robust fluorescent NPs (Ow et al. 2005).

The unique physicochemical properties of SiO_2 NPs that make them attractive for industry, however, may bring potential health hazards. Through their ability to cross biological barriers SiO_2 NPs are clearly beneficial potential tools in drug delivery systems, however, they may interfere with other physiological functions. The potential penetration of silica-coated nanomaterials through the blood brain barrier (Kim et al. 2006) and the nasal epithelium (Sundaram et al. 2009) highlights the need for comprehensive studies on their potential toxic effect on neural tissue cells. Increasing numbers of toxicological studies on SiO_2 NPs have resulted in inconsistent conclusions (Jin et al. 2007; Yang et al. 2009; Nabeshi et al. 2010; Sun et al. 2011). Many of these studies, however, have used NPs that were not fully characterized in terms of structure and physicochemical properties. As nano-specific physicochemical properties determine the interactions of NPs with living material even small differences in these properties can modulate toxicity and NPs behavior in biological solutions. Moreover, in biological media, several characteristics of NPs, including particle size/size distribution and surface chemical composition, may change. This is mainly due to NPs interactions with biomolecules (Stark 2011). Based on these considerations, the NPs used in the present study were prepared under strictly controlled conditions and were characterized with a variety of physicochemical methods both as synthesized, and also in conditions mimicking physiological environments. In addition, potential interferences of particles with the applied biological assays were carefully analyzed and the adsorption of proteins to NPs was examined.

To follow the route of NPs in living cells and tissues is a challenging task. In the present studies, fluorescent particles were used to visualize the uptake of differently functionalized SiO_2 NPs by different types of neural cells. In order to protect the encapsulated dye from leaching, the dye was covalently bound to the NP core, and a pure SiO_2 shell was synthesized onto the surface. Since the particles are to be used also for biomedical/commercial applications, the surface of fluorescent core/shell 50 nm SiO_2 NPs were further functionalized with -NH_2 and -SH groups (Ruedas-Rama et al. 2012), or were coated with polyvinylpyrrolidone (PVP), an amphiphilic, non-charged polymer, thought to reduce molecular interactions at particle surfaces (Robinson and Williams 2002).

Biological effects of these NPs were examined using primary brain cell cultures, purified microglia cells, cloned neural stem cells and their *in vitro* differentiating progenitors, by assaying metabolic activity and the rate of cell decay. Locating NPs on the surface or within neural cells was made possible by the bright fluorescence of the NPs and by using confocal microscopy in combination with fluorescence spectrum detection. High resolution spectral analysis provided a useful tool to distinguish particle-fluorescence from auto-fluorescence of cells and cell debris.

Materials and methods

NPs preparation

Highly concentrated, spherical core-shell 50 nm SiO_2 NPs encapsulating fluorescein-isothiocyanate (FITC, ≥90%, Fluka) were synthesized with a modified Stöber method (Stöber et al. 1868), (SI, NPs synthesis). The NPs surface was either coated with polyvinylpyrrolidone (PVP K-15, Sigma) or modified to generate amino and mercapto functionalities by addition of 3-aminopropyltriethoxysilane (APTES, 98%, Alfa Aesar) and 3-mercaptopropyltrimethoxysilane (MPTMS, Sigma-Aldrich) organosilanes, respectively (SI, NPs synthesis). For biological tests the NP solutions were dialyzed under sterile

conditions against 20-fold volume of minimum essential medium (MEM, Sigma) for 48 h, changing the medium 3 times.

NPs physicochemical characterization

Hydrodynamic size/size distribution of NPs and zeta potential were measured by a Brookhaven Instruments Corporation particle size analyzer (90Plus). The NP size was assessed by dynamic light scattering (DLS) using a He-Ne laser (673 nm) as the light source. The stock suspension was diluted with 99.9% ethanol to result in a count rate of 100-500 kcps. Particle sizing measurements were performed in 10 mm quartz cuvettes at 25 °C. The results were given as average values of a number, volume or intensity size distribution. The zeta potential was determined by laser Doppler electrophoresis (LDE) using a quartz capillary electrophoresis cell. All of the measurements were performed in triplicate for each batch of NPs and the results were shown as average of three measurements.

The NPs size distribution was additionally determined by a Beckman Ultracentrifuge type XL70, equipped with an optical device (AC). As the light source a diode laser (695 nm) with an optical fibre was used. A photodiode detector was connected to an analogue digital converter. For the analysis, a 3 mm Beckman quartz cell was used with a gap width of approximately 0.3 mm for the passage of light. The samples were diluted to a concentration range of 0.5-0.05%. Depending on the particle size, the samples were centrifuged for 10-120 min at speed of 4000 to 50 000 U min^{-1}.

The size and shape of primary NPs were assessed using a Phillips CM20 transmission electron microscope (TEM) working at 200 keV. For TEM analysis, stock NP suspensions were diluted 1:100 and 5 µl aliquots were pipetted onto carbon grids (S162, Plano GmbH) and subsequently left to evaporate. A series of images were selected to estimate particle size/size distribution using the analySiS pro software from Olympus.

The size and shape of primary NPs were additionally assessed using a FEI Sirion 100 T scanning electron microscope (SEM) working at 10 keV. For SEM analysis, 20 µl stock suspensions were dried directly on the carbon adhesive pad of a SEM sample holder.

The chemical and elemental composition of NPs were examined with a PHI VersaProbe 5000 scanning X-ray photoelectron spectroscope (XPS), using a monochromated Al Kα X-ray beam scanned over a 600 µm x 400 µm area (200 µm diameter/50 W X-ray beam) or 1400 µm x 100 µm (100 µm diameter/100 W X-ray beam) at a fixed take-off angle of 45°. For XPS analysis, the stock suspensions were dried on an indium surface. Spectra evaluation was performed using MultiPack-Version 9.2 software from Physical Electronics. The results in percentages were derived from relative concentrations of elements and their chemical bonds from line shape analyses.

Surface chemistry measurements were performed using a ION-TOF time-of-flight secondary ion mass spectrometer IV (ToF-SIMS). The primary ion species was 10 keV Ga^+, scanning an area of 150x150 μm^2. For SIMS analysis, the stock suspensions were dried on a gold surface.

Crystallite size and crystalline phase were evaluated by X-ray diffractometer (XRD) PANalytical EMPYREAN PIXcel with 3D Counter, operating at 40 kV voltage and 40 mA current with Cu Kα and Kβ radiation. For XRD analysis, the stock suspensions were dried on a silicon surface.

Specific surface area was determined using BET method (Brunauer et al. 1938), from nitrogen adsorption/desorption isotherms, recorded at 77 K on Gemini 2360 from Micromeritics S/N 3014. The measuring range was 0.1-1000 $m^2\ g^{-1}$. The stock solution was previously freeze dried to obtain 0.5 g of a sample.

NPs concentration was analyzed with a Mettler Toledo halogen moisture analyzer (HR73). One gram of the stock solution was placed onto analyzer plate and left for the solvent to evaporate to get a wt/wt % value.

Cell Cultures

NE-4C neuroectodermal stem cells (Schlett and Madarász 1997) (ATTC CRL-2925) were maintained in MEM supplemented with 4 mM glutamine and 10% fetal calf serum (FCS, Sigma) (MEM-FCS). NE-4C cells were differentiated into neurons (Varga et al. 2008) and astrocytes (Hádinger et al. 2009) as previously described. Primary brain cell cultures were prepared from a forebrain of 15-16 day-old mouse embryos (neuron-enriched cultures), or from 1-3 day-old postnatal mice according to Madarász et al. (1984; 1991). The cells were maintained in MEM-FCS, with medium exchange on every second day. Neuronal cultures were investigated on the 7^{th} and astroglial cultures on the 15^{th} day after plating. Microglial cultures were prepared according to Saura et al. (2003). Briefly, confluent cultures of newborn mouse brain derived glial cells were trypsinized with 0.05% (wt/v) trypsin in the presence of 0.2 mM EDTA and 0.5 mM Ca^{2+}. After detachment of astrocytes, the firmly attached microglial cells were further propagated in Dulbecco's modified Eagle's medium (DMEM, Sigma) and Ham's F12 nutrient mixture (F12, Sigma) (DMEM-F12, 1:1) with 10% FCS.

Assays on cell viability (MTT reduction) and cell death (extracellular LDH activity)

Leakage of lactate dehydrogenase (LDH) enzyme due to cell membrane damages was assessed by measuring LDH activity in cell culture media, as described previously (Kazuho and Norio 2000), with some modifications (SI, MTT and LDH assays). Metabolic activity was evaluated spectrophotometrically by measuring the reduction of tetrazolium salt 3-(4,5-dimethylthiazol-2-yl)-2,5 diphenyltetrazolium bromide (MTT) to formazan (Mosmann 1983) (SI, MTT and LDH assays).

For LDH and MTT assays, the media of cells grown in 96-well plates (10^4 cells/well) were changed to serum-free MEM-F12 medium supplemented with 1% (v/v) insulin, transferrin and selenium solution (ITS, Invitrogen) (MEM-F12-ITS), and incubated with different concentrations of NPs prepared in MEM-F12-ITS medium (100 µl total

solution/well), for 1, 24 or 48 h. The NP dispersions were placed for 10 min in a sonication bath before distribution in the culture wells. For controls, cells were incubated in MEM-F12-ITS medium (non-treated "viable" control) or in MEM-F12-ITS containing 0.01% Triton X-100 (100% damaged "death" control).

For LDH assay, 50 µl aliquots of culture medium were collected from each well, mixed with the same volume of the LDH substrate mixture and incubated for 5 min at 37 °C in CO_2 incubator. Ten microliter of MTT stock solution (2.5 mg ml^{-1}) was added to the remaining medium (50 µl) and the cells were left for 1.5 h at 37 °C in a CO_2 incubator. Both, MTT reduction and LDH reactions were stopped by adding 100 µl of solution containing 50% dimethylformamide and 20% sodium dodecyl sulfate (DMF-SDS, pH 4.7). The absorbance was measured with a BioRad microplate reader at 550 nm test and 650 nm reference wavelengths.

The interference of the NPs with LDH or MTT assays was tested in cell-free assay systems (SI, MTT and LDH assays).

Immunocytochemical and uptake studies

For microscopic analyses, cells were grown on poly-L-lysine coated glass coverslips, in 24 well plates (10^5 cells/well). The cells were incubated with 500 µl of $5x10^{11}$ NPs ml^{-1} dispersed in MEM-F12-ITS medium for 1 h at 37 ºC in a CO_2 incubator. Control cells were incubated with MEM-F12-ITS medium without NPs. The treated cells were washed three times with phosphate buffered saline (PBS, pH 7.4) to remove free-floating NPs and fixed for 20 min with paraformaldehyde (4% wt/v, PFA) at room temperature (RT).

For immunocytochemical identification, fixed cells were permeabilized with 0.1% Triton-X for 10 min at RT. Non-specific antibody binding was blocked by treating with 2% bovine serum albumin (BSA) in PBS for 60 min. Primary antibodies were diluted with 2% BSA, and fixed cells were incubated with the antibodies overnight at 4 ºC. Neurons differentiating from

NE-4C stem cells or developing in primary neuronal cultures were stained with mouse monoclonal anti-β-III tubulin antibodies (1:1000, Sigma). Astrocytes were stained with mouse monoclonal anti-glial fibrillary acidic protein (GFAP) antibodies (1:1000, Sigma). After overnight incubation, the cells were washed three times with PBS and incubated for 1 h with alexa-594 conjugated anti-mouse antibody (1:1000, Molecular probes, Invitrogen). After washing, the stained preparations were mounted with mowiol (Calbiochem, EMD Chemicals) containing 10 μg ml^{-1} bisbenzimide (Sigma) and were left to dry in dark for 24 h.

Microscopic evaluation

Cellular uptake of NPs was examined using Zeiss Axiovert 200M microscope (Carl Zeiss Microimaging) and Nikon A1R confocal laser scanning microscope (Nikon Instruments Europe B.V.) equipped with an enhanced spectral detection unit (SD) for fluorescence spectrum analysis (Heider et al. 2010).

In spectrum analysis, the samples were excited with 488 nm wavelength laser light in a Nikon A1R confocal laser scanning microscope. The emitted light was projected onto a diffracting grating in the SD, where the emitted light was separated by wavelength of 2.5 nm. In the SD unit, the spectrally separated light beams were reflected by a focusing mirror to one of the 32 photomultiplier tubes of a multi-anode photomultiplier. As a result, every pixel of a sample image had a photocurrent intensity value at each wavelength. Plotting intensity data as a function of wavelength, emission spectra for image-points were gained. The interesting spots on an image were selected by delineating the regions of interest (ROIs). The spectrum plots of ROIs were compared to positive and negative controls. The fluorescent spectra of NPs dispersed in microscopic mounting material were used as positive controls. For negative control, the auto-fluorescence spectra of corresponding regions of non-treated cells were used.

Assays on protein adsorption at NP surfaces

To investigate protein adsorption onto NPs, the NPs were dispersed in MEM supplemented with 10% fetal bovine serum (FBS). The NPs were incubated for 1 h at 37 °C in a CO_2 incubator and centrifuged for 15 min at 8000 x g. Sedimented NPs were washed with PBS to remove non-bound proteins. Bound proteins were eluted from the NPs by sodium dodecyl sulfate (SDS) (1% wt/v) washing, separated on 12% SDS-polyacrylamide gel electrophoresis (SDS-PAGE) gels and stained for 1 h in Coomassie blue, as described before (Monopoli et al. 2011). Gel electrophoresis was performed at 20 mV for about 60 min each.

Results

Synthesis and characterization of SiO_2 NPs

Fluorescent core/shell SiO_2 NPs with the desired 50 nm size were produced in very high concentration (2% wt/wt, $1.5x10^{14}$ NPs ml^{-1}) and were thoroughly characterized (Table I). SEM and TEM images showed the spherical shape and monodispersity of the NPs (Figure 1). The monodispersity was also evident in DLS and AC measurements (Figure 1). The XRD analysis spectra displayed a single broad peak indicating the amorphous nature of the SiO_2 NPs and are shown in Figure S1 in the Supplementary Material (SI). A presence of different functional groups on the NPs surfaces was indicated by XPS and ToF-SIMS analyses (SI, Figure S2 and Figure S3). TEM, DLS and zeta potential measurements highlighted the stability of the NPs after functionalization (Figure 2, Table I).

DLS analyses showed that, except for the SiO_2_PVP, all of the synthesized NPs were inclined to agglomerate/aggregate after dialysis against MEM (Table II). After 10 min of sonication, the hydrodynamic diameter of the agglomerates decreased, however, the particle size significantly differed from the size of primary NPs. Subsequent incubation in MEM-F12-ITS tissue culture media increased the agglomeration rate (Table II). The agglomeration depended on the incubation time, surface functionalization and the concentration of the NPs (SI, Figure S4 and Figure S5).

Effects of SiO_2 NPs on survival and metabolic activity of different neural tissue-type cells

In LDH cytotoxicity assays and MTT cell metabolism tests, incubation with the NPs for 4 or 24 h did not cause significant changes. However, after 48 h exposure marked differences were found among the effects of the NPs depending on the surface chemistry and the dose of the NPs, and also on the type of the cells (Figure 3).

Potential interactions of the NPs with assay-components were checked in cell-free MTT and LDH assays. As it is shown in Figure S6 (SI), none of the particles interfered with the tests.

In MTT assays, NE-4C neural stem cells showed reduced viability only at very high (2 mg ml^{-1}, $1x10^{13}$ NPs ml^{-1}) concentration of the NPs. In comparison to non-treated cells (100% viability), viability decreased significantly in the presence of the plain SiO_2 NPs (37% ± 19), SiO_2_NH_2 (51% ± 20) and SiO_2_SH (70% ± 13), while did not change if the cells were exposed to the PVP-coated NPs (Figure 3-A).

LDH tests indicated cell membrane damage at ten times lower NPs concentration (0.2 mg ml^{-1}, $1x10^{12}$ NPs ml^{-1}), an almost equal toxicity of the plain SiO_2 NPs (152% ± 19), SiO_2_SH (142% ± 17) and SiO_2_NH_2 (141% ± 14) was shown, while effects of the SiO_2_PVP particles were not detected when compared to non-treated cells (100%). The SiO_2_PVP NPs had no effect even at the highest (2 mg ml^{-1}) concentration, while the other NPs increased the LDH release more than two times (SiO_2: 282% ± 19, SiO_2_NH_2: 269% ± 46, SiO_2_SH: 206% ± 19) (Figure 3-B).

The viability of NE-4C-derived neurons was slightly decreased (MTT-reduction) only in response to the plain SiO_2 NPs at high (0.2 and 2 mg ml^{-1}) concentrations (80% ± 7 and 78% ± 4, respectively) (Figure 3-C). LDH test again proved to be more sensitive - responses by neurons were also found with exposure to the SiO_2_NH_2 NPs (at 2 mg ml^{-1}: 131% ± 5)

(Figure 3-D). The data showed some enhanced sensitivity of non-differentiated neural stem cells in comparison to their *in vitro* differentiated neural derivatives.

Lower sensitivity of more mature neural cells was also indicated by data obtained on primary brain cell cultures containing both neurons and astrocytes (Figure 3-E and Figure 3-F). In these cultures, only bare SiO_2 NPs caused detectable damages and only at high concentrations.

Microglial cells isolated from postnatal mouse brain were slightly damaged by SiO_2, SiO_2_NH_2, and SiO_2_SH NPs, but not by PVP-coated NPs (SI, Figure S7).

Uptake studies

Incubation with 500 µl of $5x10^{11}$ NPs ml^{-1} (dispersed in MEM-F12-ITS medium) did not result in obvious structural damages of cells compared to untreated controls. To obtain information about the uptake of the plain SiO_2, SiO_2_NH_2, SiO_2_SH and SiO_2_PVP NPs by different neural cells, confocal microscopic studies were conducted on NE-4C neural stem cells, on primary brain cell cultures enriched in neurons or in astrocytes, on purified microglial cells and on co-cultures of astrocytes and microglia.

For microscopic visualization, NPs were accessible only if agglomerated in solutions, accumulated on cell surfaces or collected into the endo/lysosome compartments of cells. In culture media, plain SiO_2, SiO_2_NH_2 and SiO_2_SH NPs formed large, light microscopically detectable agglomerates. In 1 h exposure time, the agglomerates settled on cell surfaces and on the glass substrate, and could not be removed with multiple washing. The SiO_2_PVP NPs, on the other hand, were hardly visible by conventional fluorescence microscopy on the outside of the cells, reinforcing the DLS data on reduced agglomeration of NPs after PVP functionalization.

To distinguish NP fluorescence from the auto-fluorescence of cells and cell debris, the spectrum of non-treated control cells (negative control) and the emission spectrum of NPs

(positive control) were compared to spectra of regions of interest (ROIs) chosen by either random selection or targeted sorting of microscopically visible fluorescence spots (SI, Figure S8). To decide whether the analyzed fluorescence spots were inside or outside the cells, confocal z-stack analysis was performed.

After 1 h incubation with the plain SiO_2, SiO_2_NH_2 or SiO_2_SH NPs, particle-derived fluorescence was found in or on the surface of NE-4C neural stem cells (Figure 4), astrocytes (Figure 5) and microglial cells (Figure 6), but not in neurons (Figure 7).

Incubation with the SiO_2_PVP NPs, on the other hand, did not result in accumulation of particle-delivered fluorescence in any cells including microglia. Z-stack analyses demonstrated that microglia cells internalized the plain SiO_2, SiO_2_NH_2 and SiO_2_SH NPs but not the SiO_2_PVP NPs (Figure 6). Astrocytes, while carrying the plain SiO_2, SiO_2_NH_2 and SiO_2_SH NPs on the cell surface, engulfed only a small amount of NPs, and did not take up the SiO_2_PVP NPs at all (Figure 5). In 1 h exposure time, primary neurons did not take up detectable amount of any NPs (Figure 7). NE-4C neural stem cells, on the other hand, engulfed the plain SiO_2, SiO_2_NH_2 and SiO_2_SH NPs, but did not show intracellular fluorescence after exposure to the PVP-coated NPs (Figure 4).

The low aggregation in physiological solutions and the minimal cellular uptake of SiO_2_PVP NPs indicated that the PVP coat could highly reduce the surface-activity of the SiO_2 NPs. The assumption was checked by investigating the composition of the protein layer absorbed on the surface of differently functionalized SiO_2 NPs.

Absorption of serum proteins by differently functionalized silica nanoparticles

Plain SiO_2, SiO_2_NH_2, SiO_2_SH and SiO_2_PVP NPs were incubated with physiological solutions containing 10 % FBS for 1 h. After rigorous washing, the NPs were dispersed in SDS containing buffer and loaded onto poly-acrylamide gel for electrophoretic analysis of adsorbed proteins. The protein bands (Figure 8) indicated that the plain SiO_2, SiO_2_NH_2 and

SiO_2_SH NPs adsorbed a variety of proteins, while the SiO_2_PVP NPs carried a single protein component with 66-68 kDa molecular weight, corresponding to albumin, the most abundant serum protein. The PVP coat significantly reduced the total mass of absorbed proteins on the NPs surfaces.

Discussion

The aim of the study was to investigate responses of different neural tissue-type cells to 50 nm fluorescent core/shell SiO_2 NPs with different surface functionalization. For this reason, highly monodispersed SiO_2 NPs were synthesized in a concentration which allowed performing tests in a broad range, from 0.2 µg ml^{-1} (10^9 NPs ml^{-1}) to 2 mg ml^{-1} (10^{13} NPs ml^{-1}). In order to protect encapsulated dye molecules from external influences or from leaching, the dye was covalently bound within a silica core and a pure silica shell was synthesized onto the NP surface. The surface of NPs was further functionalized with -NH_2, -SH groups or coated with PVP.

Since it is known that biological activity of NPs depends on physico-chemical parameters, proper and accurate NPs characterization is a basic requirement for understanding biological effects and for providing reproducibility. Conflicting nanotoxicological data might find explanation if detailed characterization of applied NPs had been known. Nevertheless, as it has been recognized by leading researchers (Oberdörster et al. 2010), full NPs characterization has not always been considered in toxicity screening, mainly because of the complexity of the required assays. Full characterization of NPs should ideally include multiple measurements of particle size and size distribution, agglomeration state, shape and morphology, crystallinity, composition, surface chemistry and charge, and surface area. Almost each characteristic should be measured by more than one method, because of technique limitations, assay interference or specific requirements of sample preparation. NPs used in the presented investigations were strictly characterized using a variety of

physicochemical methods including zeta potential, DLS, TEM, SEM, AC, BET, XPS, ToF-SIMS and XRD.

Furthermore, many NPs are likely to undergo significant size distribution or surface changes while transferred between media. Thus, NPs characteristics should be checked after incubation in biological solutions. Since small changes in NPs characteristics may modify their cellular uptake and intracellular reactivity (Xia et al. 2008) serial monitoring of NPs features were included in this study, in accordance with recent trends in nanotoxicology (Horie et al. 2009; Ehrenberg et al. 2009; Zhu et al. 2009).

In biological media including protein-free physiological buffer solutions the plain SiO_2, SiO_2_NH_2, and SiO_2_SH NPs rapidly agglomerated indicating that the ionic strength and concentration of the main body fluids evoked fundamental changes in basic NP features. The rate of agglomeration and size of the agglomerates made questionable whether the detected biological effects could be attributed to "nano"-effects. The PVP-coat prevented the formation of micron-size agglomerates, and accordingly, rapid sedimentation. The SiO_2_PVP particles did not settle in large agglomerates on cell surfaces which might be a reason behind their lower biological activity and reduced cellular uptake.

Cytotoxicity (LDH) and cell viability (MTT) assays demonstrated that plain SiO_2, SiO_2_NH_2, and SiO_2_SH NPs exerted some cell damage, but only at very high NPs doses (2 mg ml^{-1} and 0.2 mg ml^{-1}), which exceed any realistic dose (Gangwal et al. 2011). The SiO_2_PVP NPs, on the other hand, did not evoke measurable effects on any of the investigated neural cells. Besides surface chemistry, the toxic dose of NPs depended also on the type of exposed cells. NE-4C neural stem cells seemed to be more sensitive than either NE-4C-derived or primary (brain tissue-derived) neurons. Microglial cells displayed a relatively large (40%) increase in LDH release in response to high doses ($1x10^{12}$ ml^{-1}) of SiO_2, SiO_2_NH_2, and SiO_2_SH NPs, which was similar in magnitude to the reaction of stem cells. The data suggested some enhanced vulnerability for developing neural tissue known to

contain elevated numbers of stem/progenitor cells, and also for degenerating/regenerating brain tissue regions characterized by increased proportions of both non-differentiated progenitor-type cells and microglia.

To correlate toxicity data with the uptake of various NPs, the non-leaky fluorescence of SiO_2 core/shell NPs was monitored by microscopic techniques. In traditional fluorescence microscopy, individual NPs cannot be visualized, individual light-emitting particles may provide a stain-like fluorescence if present in high density, but single NPs scattered sporadically on microscopic fields are beyond the resolution of fluorescence microscopy. Agglomerates of NPs, by providing larger area and intensity of light emission, however, can be easily resolved. Active cellular internalization collects the NPs in endocytotic vesicles, a cellular process which helps to localize actively internalized fluorescent NPs. Fixed or fresh tissue sections and cells, however, also emit light if excited with illumination at wavelengths which commonly used to excite conventional fluoroprobes. This background fluorescence should be distinguished from NP-fluorescence in order to "see" NPs in biological samples. If the emitted light spectrum of autofluorescence differs from that of NPs, fluorescence spectrum analysis can demonstrate the presence of particles even if traditional fluorescence microscopy does not allow selective imaging (Dickinson et al. 2001; Haraguchi et al. 2002). Combining fluorescence spectrum analysis with confocal Z-stack analysis, cellular localization of fluorescent NPs with different surface functionalization was determined and compared. Microscopic studies showed that the surface membranes of neurons did not attract agglomerated NPs, and neurons did not take up the NPs, regardless of surface functionalization. On the surface of neural stem cells and astrocytes, all NPs, except those with PVP-coating, accumulated in large agglomerates but only a few were internalized. As it was expected, microglial cells, the resident macrophage cells of the central nervous system (CNS), took up large amounts of the plain SiO_2, SiO_2_NH_2, and SiO_2_SH NPs in 1 h exposure time, but active uptake of the SiO_2_PVP NPs was not detected even in these cells. While the

applied methods could not provide data on scattered permeation of single NPs, they clearly demonstrated that PVP-coating decreased the agglomeration of NPs in biological solutions, prevented the accumulation of NPs on cell surfaces and diminished the endocytotic uptake of NPs. Gel electrophoresis analysis of serum proteins absorbed on particle surfaces revealed that the PVP coat reduced “protein corona” formation. The results indicated that surfaces of the 50 nm SiO_2 NPs could be biochemically ”inactivated” by non-covalent covering with PVP.

As PVP (once used as a blood plasma expander) is regarded as a harmless, non-barrier-invasive material, and has been used as a vehicle for many pharmaceutical preparations (Bühler 2005), it may find applications in nanomedicine as well. While we are aware that *in vitro* data provides only limited information on the potential health hazards of NPs, we hope that the presented study may contribute to improved production, characterization and application of fluorescent silica NPs. *In vivo* studies on the penetration of characterized SiO_2 NPs through biological interfaces are in progress and will supplement the presented *in vitro* observations.

Conclusions

This study calls attention to the significance of surface chemistry of SiO_2 NPs in assessment of biological effects and to the standardization of cellular subjects of such evaluations. Conflicting results on safety and/or health hazard of SiO_2 NPs might be resolved by using sufficiently characterized NPs in standard procedures on defined biological subjects. The possible penetration of SiO_2 NPs through the blood-brain barrier requires strict assessment of any potential neurotoxic effects. Our *in vitro* studies show that NPs with different surface modifications exert different cellular responses, and different neural cell-types respond differently to the same NPs. The data also indicate that 50 nm fluorescent core/shell SiO_2 NPs are not considerably toxic, and that PVP coating further reduces toxic effects and cellular

uptake of NPs. Using appropriate optical detection methods, fluorescent NPs can be imaged within cells and on cell surfaces: fluorescence spectrum analysis combined with optical slicing may open ways for a variety of studies. Results of on-going *in vivo* studies will provide critical information for potential biomedical applications of fluorescent SiO_2 NPs.

Acknowledgements

The authors wish to thank the Nikon Microscopy Center at IEM, Nikon Austria GmbH and Auro-Science Consulting Ltd for kindly providing microscopy support, and Dr. Matthew Boyles for helpful comments and suggestions.

Declaration of Interest: This study was supported by the EU 7th framework programme, Marie Curie Actions, Network for Initial Training NanoTOES (PITN-GA-2010-264506), www.nanotoes.eu. The authors report no conflict of interest. The authors alone are responsible for the content and writing of the paper.

References

Brunauer S, Emmett PH, Teller E. 1938. Adsorption of gases in multimolecular layers. J Am Chem Soc 60:309-319.

Bühler V. (2005). Excipients for Pharmaceuticals - Povidone, Crospovidone and Copovidone. Heidelberg, Germany: Springer.

Dickinson ME, Bearman G, Tille S, Lansford R, Fraser SE. 2001. Multi-spectral imaging and linear unmixing add a whole new dimension to laser scanning fluorescence microscopy. BioTechniques 31(6):1272-1278.

Ehrenberg MS, Friedman AE, Finkelstein JN, Oberdörster G, McGrath JL. 2009. The influence of protein adsorption on nanoparticle association with cultured endothelial cells. Biomaterials 30:603-610.

Gangwal S, Brown JS, Wang A, Houck KA, Dix DJ, Kavlock RJ, Hubal EAC. 2011. Informing selection of nanomaterial concentrations for ToxcCast *in vitro* testing based on occupational exposure potential. Environ Health Perspec 119(11):1539–1546.

Hádinger N, Varga B, Berzsenyi S, Környei Zs, Madarász E, Herberth B. 2009. Retinoic acid regulates astrogliogenesis. Int J Devl Neurosci 27:365-375.

Haraguchi T, Shimi T, Koujin T, Hashiguchi N, Hiraoka Y. 2002. Spectral imaging fluorescence microscopy. Genes Cells 7:881–887.

Heider EC, Barhoum M, Peterson EM, Schaefer J, Harris JM. 2010. Identification of single fluorescent labels using spectroscopic microscopy. Appl Spectr 64:37-45.

Hirsch LR, Stafford RJ, Bankson JA, Sershen SR, Rivera B, Price RE, Hazle JD, Halas NJ, West JL. 2003. Nanoshell-mediated near-infrared thermal therapy of tumors under magnetic resonance guidance. Proc Natl Acad Sci USA 100:13549-13554.

Horie M, Nishio K, Fujita K, Endoh S, Miyauchi A, Saito Y, Iwahashi H, Yamamoto K, Murayama H, Nakano H Nanashima N, Niki E, Yoshida Y. 2009. Protein adsorption of ultrafine metal oxide and its influence on cytotoxicity toward cultured cells. Chem Res Toxicol 22(3):543-53.

Jin Y, Kannan S, Wu M, Zhao JX. 2007. Toxicity of luminescent silica nanoparticles to living cells. Chem Res Toxicol 20:1126-1133.

Kazuho A, Norio M. 2000. Measurement of cellular 3-(4, 5-dimethylthiazol-2-yl)-2,5-diphenyltetrazolium bromide (MTT) reduction activity and lactate dehydrogenase release using MTT. Neurosci Res 38:325–329.

Kim JS, Yoon TJ, Yu KN, Kim BG, Park SJ, Kim HW, Lee KH, Park SB, Lee JK, Cho MH. 2006. Toxicity and tissue distribution of magnetic nanoparticles in mice. Toxicol Sci 89:338-347.

Madarász E, Theodosis DT, Poulain DA. 1991. In vitro formation of type 2 astrocytes derived from postnatal rat hypothalamus or cerebral cortex. Neuroscience 43:211–221.

Madarász E, Kiss J, Bartók I. 1984. Cell production and morphological pattern formation in primary brain cell cultures. Brain Res 304:339-349.

Monopoli MP, Walczyk D, Campbell A, Elia G, Lynch I, Baldelli-Bombelli F, Dawson KA. 2011. Physico-chemical aspects of protein corona: relevance to in vitro and in vivo biological impacts of nanoparticles. JACS 133:2525-2534.

Mosmann T. 1983. Rapid colorimetric assay for cellular growth and survival: application and proliferation and cytotoxicity assays. J Immunol Methods 65:55-63.

Nabeshi H, Yoshikawa T, Matsuyama K, Nakazato Y, Arimori A, Isobe M, Tochigi S, Kondoh S, Hirai T, Akase T, Yamashita T, Yamashita K, Yoshida T, Nagano K, Abe Y,

Yoshioka Y, Kamada H, Imazawa T, Itoh N, Tsunoda S, Tsutsumi Y. 2010. Size-dependent cytotoxic effects of amorphous silica nanoparticles on Langerhans cells. Pharmazie 65:199-201.

Oberdörster G, Maynard A, Donaldson K, Castranova V, Fitzpatrick J, Ausman K, Carter J, Karn B, Kreyling W, Lai D, Olin S, Monteiro-Riviere N, Warheit D, Yang H. 2005. Principles for characterizing the potential human health effects from exposure to nanomaterials: elements of a screening strategy. Part Fibre Toxicol 2:8.

Ow H, Larson DR, Srivastava M, Baird BA, Webb WW, Wiesner U. 2005. Bright and stable core-shell fluorescent silica nanoparticles. Nano Lett 5:113-117.

Ravi Kumar MNV, Sameti M, Mohapatra SS, Kong X, Lockey RF, Bakowsky U, Lindenblatt G, Schmidt CH, Lehr M. 2004. Cationic silica nanoparticles as gene carriers: synthesis, characterization and transfection efficiency *in vitro* and *in vivo*. J Nanosci Nanotechnol 4:876-881.

Robinson S, Williams PA. 2002. Inhibition of protein adsorption onto silica by polyvinylpyrrolidone. Langmuir 18(23):8743–8748.

Ruedas-Rama MJ, Walters JD, Orte A, Hall EAH. 2012. Fluorescent nanoparticles for intracellular sensing: a review. Anal Chim Acta 751:1-23.

Saura J, Tusell JM, Serratosa J. 2003. High-yield isolation of murine microglia by mild trypsinization. Glia 44:183–189.

Schlett K, Madarász E. 1997. Retinoic acid induced neural differentiation in a neuroectodermal cell line immortalized by p53 deficiency. J Neurosci Res 47:405-15.

Slowing II, Vivero-Escoto JL, Wu CW, Lin VS. 2008. Mesoporous silica nanoparticles as controlled release drug delivery and gene transfection carriers. Adv Drug Deliv Rev 60:1278-1288.

Stark WJ. 2011. Nanoparticles in biological systems. Angew Chem Int Ed Engl 50(6):1242-58.

Stöber W, Fink A, Bohn EJ. 1868. Controlled growth of monodisperse silica spheres in the micron size range. J Colloid Interface Sci 26:62–69.

Sun L, Li Y, Liu X, Jin M, Zhang L, Du Z, Guo C, Huang P, Sun Z. 2011. Cytotoxicity and mitochondrial damage caused by silica nanoparticles. Toxicol In Vitro 25(8):1619-29.

Sundaram S, Roy SK, Ambati BK, Kompella UB. 2009. Surface functionalized nanoparticles for targeted gene delivery across nasal respiratory epithelium. FASEB J 23(11):3752–3765.

Varga B, Hádinger N, Gócza E, Dulberg V, Demeter K, Madarász E, Herberth B. 2008. Generation of diverse neuronal subtypes in cloned populations of stem-like cells. BMC Devl Biol 8:89-107.

Vijayanathan V, Thomas T, Thomas TJ. 2002. DNA nanoparticles and development of DNA delivery vehicles for gene therapy. Biochemistry 41:14085-14094.

Walcarius A, Ganesan V. 2006. Ion-exchange properties and electrochemical characterization of quaternary ammonium-functionalized silica microspheres obtained by the surfactant template route. Langmuir 22:469–77.

Xia T, Kovochich M, Liong M, Zink JI, Nel AE. 2008. Cationic polystyrene nanosphere toxicity depends on cell-specific endocytic and mitochondrial injury pathways. ACS Nano 2:85-96.

Yang H, Wu Q, Tang M, Kong L, Lu Z. 2009. Cell membrane injury induced by silica nanoparticles in mouse macrophage. J Biomed Nanotechnol 5:528-535.

Zhu Y, Li W, Li Q, Li Y, Li Y, Zhang X, Huang Q. 2009. Effects of serum proteins on intracellular uptake and cytotoxicity of carbon nanoparticles. Carbon 47:1351-1358.

Legends and captions for figures

Figure 1. Spherical shape and monodispersity of SiO_2 NPs are evident in (A) SEM, (B) TEM, (C) DLS and (D) AC analyses.

Figure 2. TEM (A, C, E) and DLS (B, D, F) analyses of SiO_2 NPs functionalized with amino groups (SiO_2_NH_2) (A, B), with mercapto groups (SiO_2_SH) (C, D) and with

polyvinylpyrrolidone (SiO_2_PVP) (E, F) highlighted the stability of the NPs after their functionalization.

Figure 3. MTT (A), (C), (E) and LDH assays (B), (D), (F) for different neural tissue-type cells: (A), (B) NE-4C stem cells, (C), (D), NE-4C derived neurons, (E), (F) primary neuron-enriched brain cell cultures; P: "death" control (0.1% Triton X-100 treated cells); N: non-treated cells.

Figure 4. Cloned embryonic neuroectodermal stem cells (NE-4C) strongly interact with plain SiO_2 NPs (B), while almost no interaction is detected with SiO_2_PVP NPs. Spectral analyses (lower panels on A, B, C) show particle-specific fluorescence for SiO_2 NPs-treated cells (B), but not for non-treated (A) or SiO_2_PVP-treated cells.

Figure 5. Confocal images of embryonic mouse forebrain astrocytes cultured 15 days (A) and treated with SiO_2 (B) or SiO_2_PVP NPs. After 1 h exposure, SiO_2 NPs adsorb onto astrocyte surfaces, while SiO_2_PVP are easily washed out. Red: astrocytes stained for GFAP; blue: cell nuclei stained with DAPI Hoechst stain; green: fluorescent SiO_2 NPs.

Figure 6. SiO_2 NPs are internalized by microglia cells (B), while SiO_2_PVP NPs are rarely found inside the cells. For non-treated microglia cells (A) NP-specific fluorescence is not detected.

Figure 7. Confocal images of embryonic mouse forebrain neurons cultured 15 days (A) and treated with SiO_2 (B) or SiO_2_PVP NPs. After 1 h exposure, neurons do not internalize any of SiO_2 NPs. Red: neurons stained for neuron-specific tubulin; blue: cell nuclei stained with DAPI Hoechst stain; green: fluorescent SiO_2 NPs.

Figure 8. SDS-PAGE analyses of biomolecules (FBS) absorbed on NPs surfaces reveal that the PVP coat reduces ‘protein corona’ formation; M: proteins marker.

Table 1. Physico-chemical characterization of NPs

Name	SiO_2	SiO_2_NH_2	SiO_2_SH	SiO_2_PVP
Shape	spherical			
Crystal structure	amorphous			
Concentration	2.0% (wt/wt), $1.5*10^{14}$ NPs ml^{-1}			
Specific surface area	$8.31*10^{1}$ m^2/g	-	-	-
Size/size distribution & aggregation/ agglomeration state	DLS: 52.5 ± 2.6 nm [a]; PDI= 0.055 TEM: d_{50}= 50 nm, d_{90}= 55 nm AC: d_{50}= 49 nm, d_{90}= 61 nm	DLS: 56.0 ± 4.6 nm [a]; PDI=0.082 TEM: d_{50}= 51 nm, d_{90}= 58 nm	DLS: 49.9 ± 2.2 nm [a]; PDI= 0.067 TEM: d_{50}= 49 nm, d_{90}= 57 nm	DLS: 59.5 ± 2.3 nm [a]; PDI= 0.079 TEM: d_{50}= 51 nm, d_{90}= 57 nm
Surface chemistry	XPS: Atom% O 62.8, Si 25.6, C 11.6 SIMS: Si_xO_y, $C_6H_{15}O_3Si$	XPS: Atom% O 57.8, Si 24.3, C 16.1, N 1.8 SIMS: Si_xO_y, $(H_2N(CH_2)_3Si(OC_2H_5)_3)$, F	XPS: Atom% O 61.8, Si 25.6, C 12.6, S< 1 SIMS: Si_xO_y, $((CH_3O)_3Si(CH_2)_3SH)$, Cl	XPS: Atom% O 44.5, Si 33.5, C 18.0, N 3.9 SIMS: Si_xO_y, C_6H_9NO, F
Surface charge	- 41.71 mV ± 0.82 IEP: ~ pH 3.1	+ 42.24 mV ± 1.49 IEP: ~ pH 6.4	- 47.73 mV ± 0.91 IEP: ~ pH 1.3	- 40.87 mV ± 1.31 IEP: ~ pH 4.6

[a] *Z*-average hydrodynamic diameter extracted by Cumulants analysis of the data

Table 2. DLS analyses show that, except for SiO_2_PVP all of the SiO_2 NPs are inclined to agglomerate/aggregate in biological media.

	Size [nm]			
	SiO_2	SiO_2_NH_2	SiO_2_SH	SiO_2_PVP
MEM (48 h; RT; $1x10^{14}$ NPs mL^{-1})	1626 ± 260	1892 ± 423	1844 ± 818	67 ± 4
MEM-sonication 10 min (48 h; RT; $1x10^{14}$ NPs mL^{-1})	785 ± 156	873 ± 199	932 ± 176	65 ± 3
MEM-F12-ITS (1 h; 37°C; $5x10^{11}$ NPs mL^{-1})	1119 ± 62	976 ± 163	1247 ± 137	68 ± 6

Supplementary Material

NPs synthesis

In a first step, the fluorescent cores were prepared by hydrolysis and condensation of tetraethyl orthosilicate (TEOS, ≥99.0%, Sigma-Aldrich) in absolute ethanol (≥99.8%, Sigma-Aldrich) and presence of ammonium hydroxide (NH_4OH, 26 %, Riedel-de Haën) as a catalyst and fluorescein-isothiocyanate (FITC, ≥90%, Fluka) as a fluorescent dye. FITC was previously reacted with 3-aminopropyltriethoxysilane (APTES, 98 %, Alfa Aesar) in ethanol (in molar ratio 10:1) for 24 h, in order to covalently incorporate the dye into the NPs, and 70 µl of the reaction product was subsequently mixed with solution containing 100 g of the absolute ethanol, 5 g of NH_4OH and 4.7 g of TEOS. The reaction proceeded at ambient temperature for 24 h in dark. Afterwards, the colloids were dialyzed in cellulose membrane (14 kDa, Roth) against the absolute ethanol to remove an excess of the reagents.

In the second step, the pure silica shells were synthesized. To 100 g of silica cores solution 5 g of NH_4OH was added and subsequently 4.7 g of TEOS. The reaction proceeded at ambient temperature for 24 h. Thereafter, the core/shell NPs were dialyzed against the absolute ethanol.

For the amino functionalization, pH of the synthesized core/shell NPs colloidal solution (30ml) was adjusted to 5.9 and 1500 µl of APTES was added. To generate mercapto functionalization, 2100 µl of MPTMS was stirred with 30 ml of core/shell NPs solution. SiO_2 NPs were also coated with polyvinypyrrolidone (PVP, K-15, Sigma- Aldrich) by mixing 30 ml of cores solution with 0.3 g PVP, 0.5 g NH_4OH and 0.47 g TEOS. All functionalized NPs were stirred at RT for 12 h and thereafter dialyzed against absolute ethanol.

MTT and LDH assays

MTT was dissolved in phosphate-buffered saline (PBS, pH 7.4) at a concentration of 2.5 mg ml^{-1} (6 mM), and stored at 4 °C. 1-methoxy-5-methylphenazinium methylsulfate (MPMS, Sigma) was dissolved in PBS at a concentration of 100 mM, and stored at 4 °C. Lactate dehydrogenase (LDH) substrate mixture (1 ml) was prepared as follows; 2.5 mg L-lactate salt and 2.5 mg nicotinamide adenine dinucleotide (NAD, Sigma) were dissolved in 0.9 ml of 0.2 M Tris–HCl buffer (pH 8.2) and 0.1 ml of MTT stock solution and 1 µl of MPMS stock solution were added.

We have demonstrated that both MTT reduction (an index of cellular activity) and LDH release (an index of cell membrane damage) can be measured using MTT conversions. MTT assay measures the conversion of MTT into purple-colored MTT formazan by the redox activity of living cells, and a decrease in cellular MTT reduction could be an index of cell damage. On the other hand, LDH assay measures the release of the intracellular enzyme LDH upon damage of the plasma membrane, and an increase in LDH release could be an index of cell damage.

Bovine LDH (Sigma-Aldrich Chemie GmbH, Munich) was used to determine the influence of NPs dispersions on LDH activity. NPs dispersions in MEM-F12-ITS were mixed with 2 U ml^{-1} LDH in cell-free wells (100 µl/well) and incubated for 48 h at 37 °C in a CO_2 incubator. Supernatants (50 µl) were transferred to new 96-well plates, and 50 µ of the LDH assay solution was added. The absorbance was measured with a microplate reader at a test wavelength of 550 nm, and a reference wavelength of 650 nm.

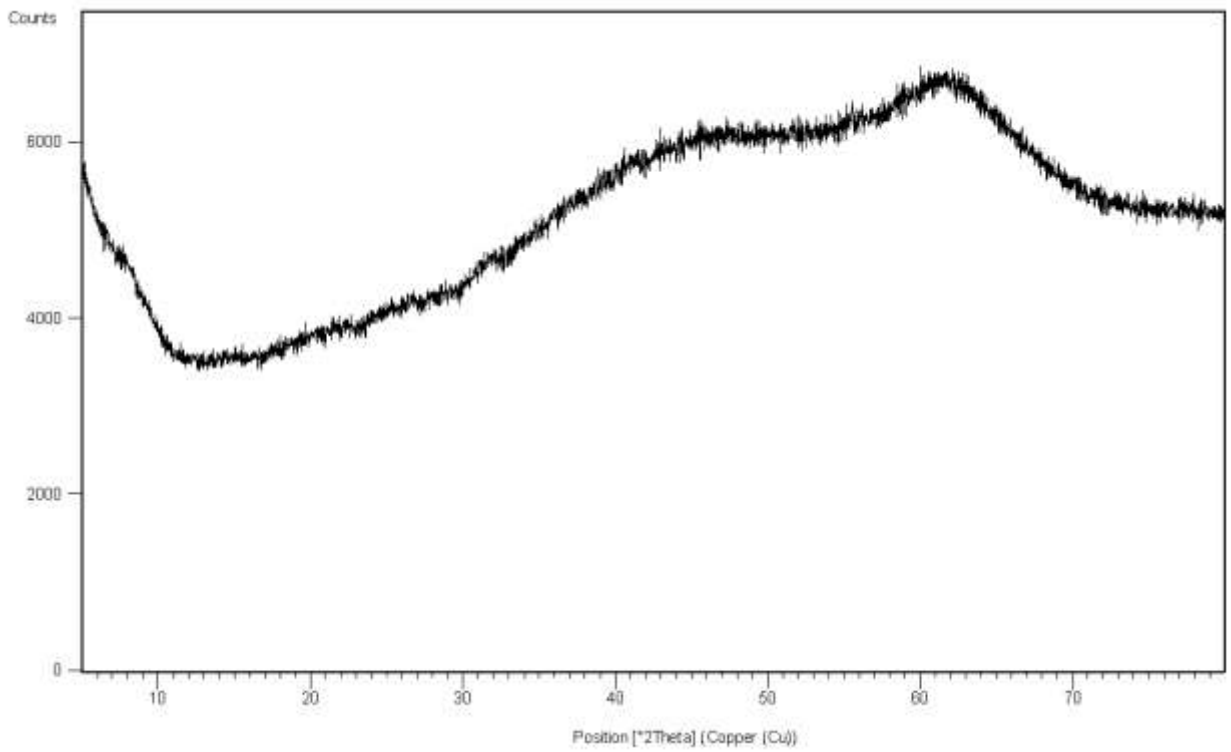

Figure S1. XRD analysis of SiO_2 NPs showing their amorphous form.

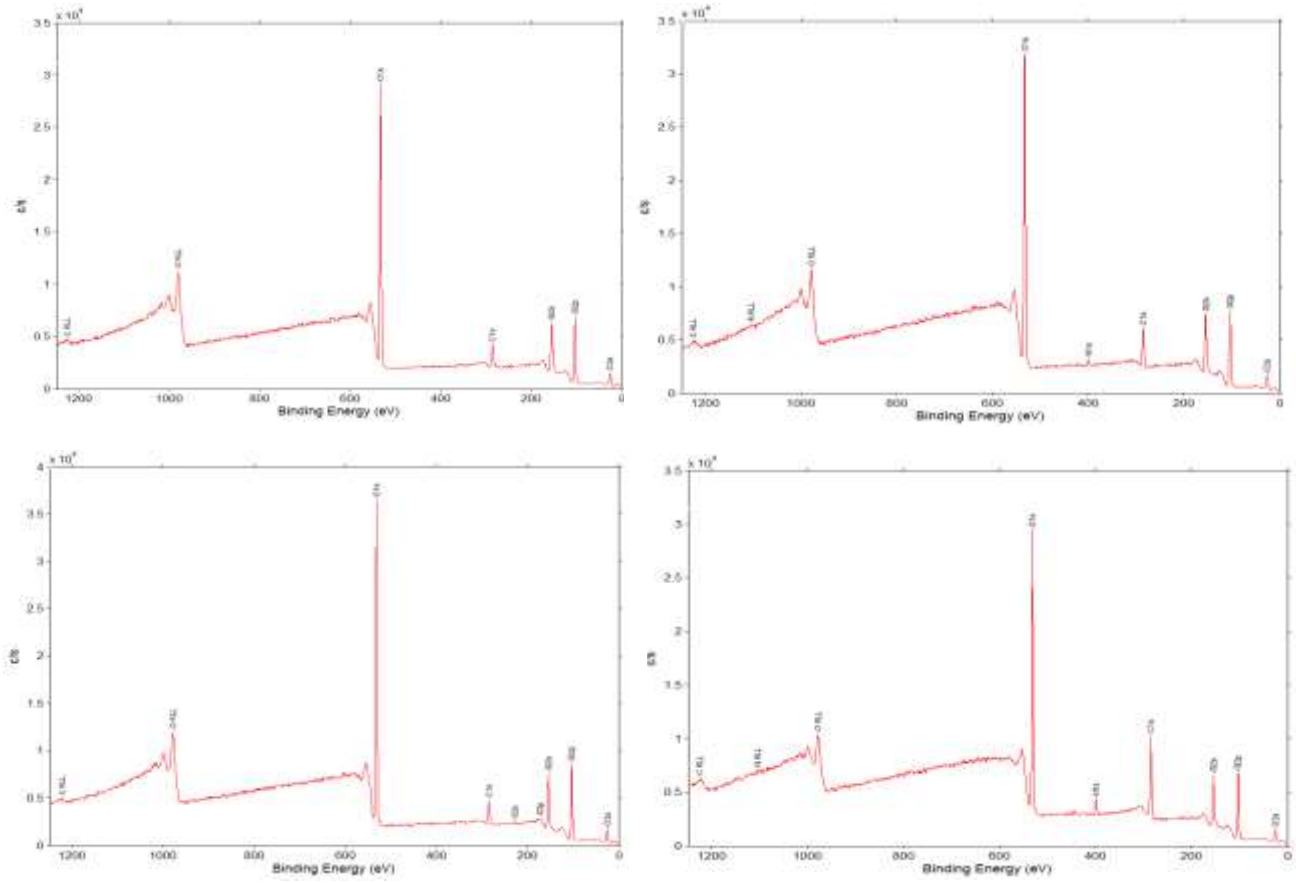

Figure S2. XPS analysis of not functionalized particles (a) SiO_2 and after functionalization (b) SiO_2_NH_2, (c) SiO_2_SH, (d) SiO_2_ PVP.

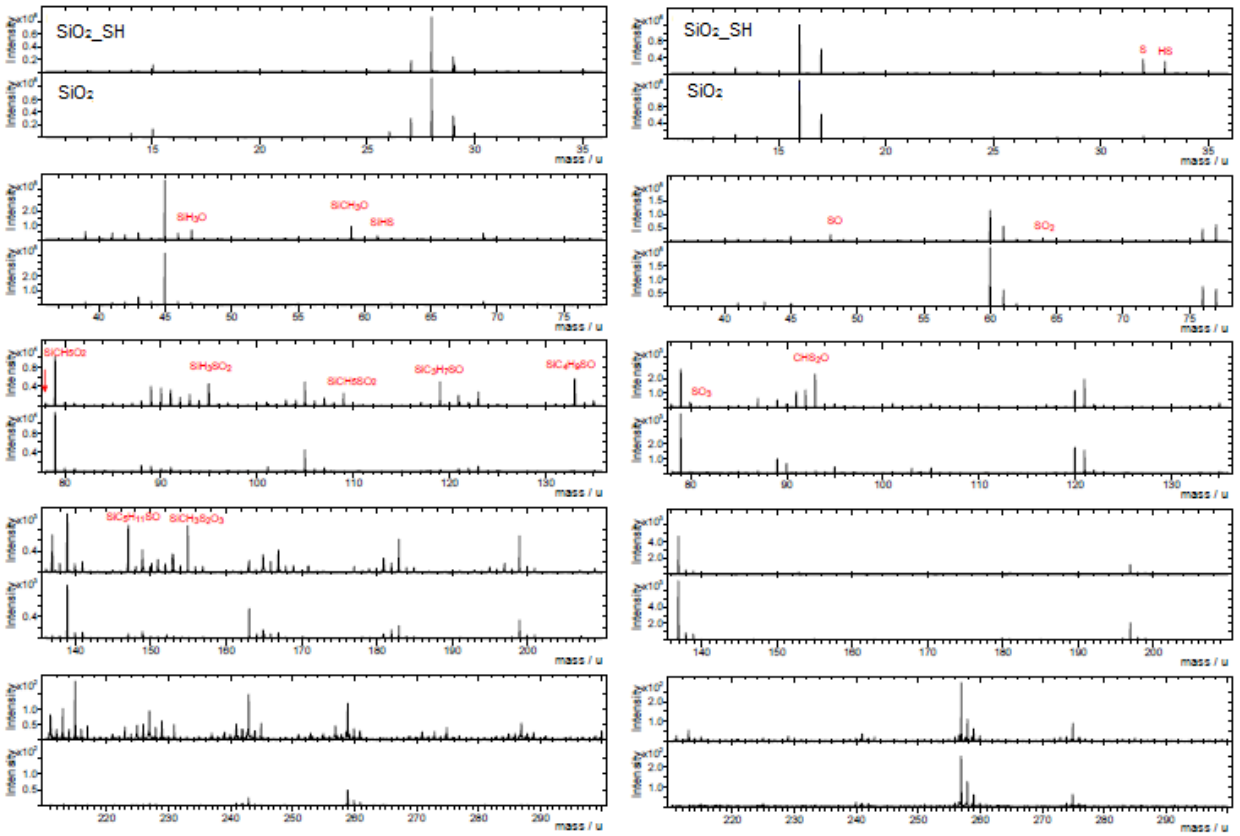

Figure S3-A. ToF-SIMS analysis for (a) SiO_2_NH_2 in comparison to not functionalized SiO_2 NPs obtained from positive (left) and negative (right) polarity.

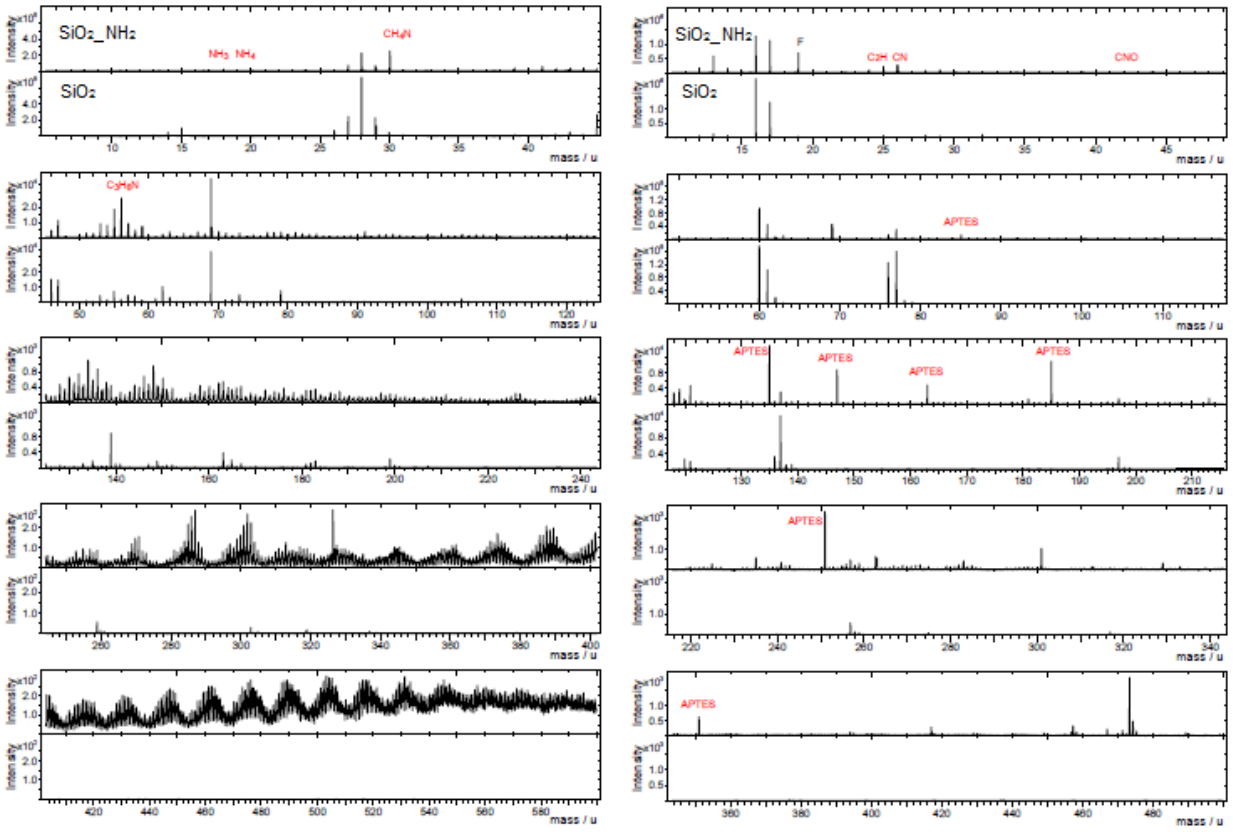

Figure S3-B. ToF-SIMS analysis for (b) SiO_2_SH in comparison to not functionalized SiO_2 NPs obtained from positive (left) and negative (right) polarity.

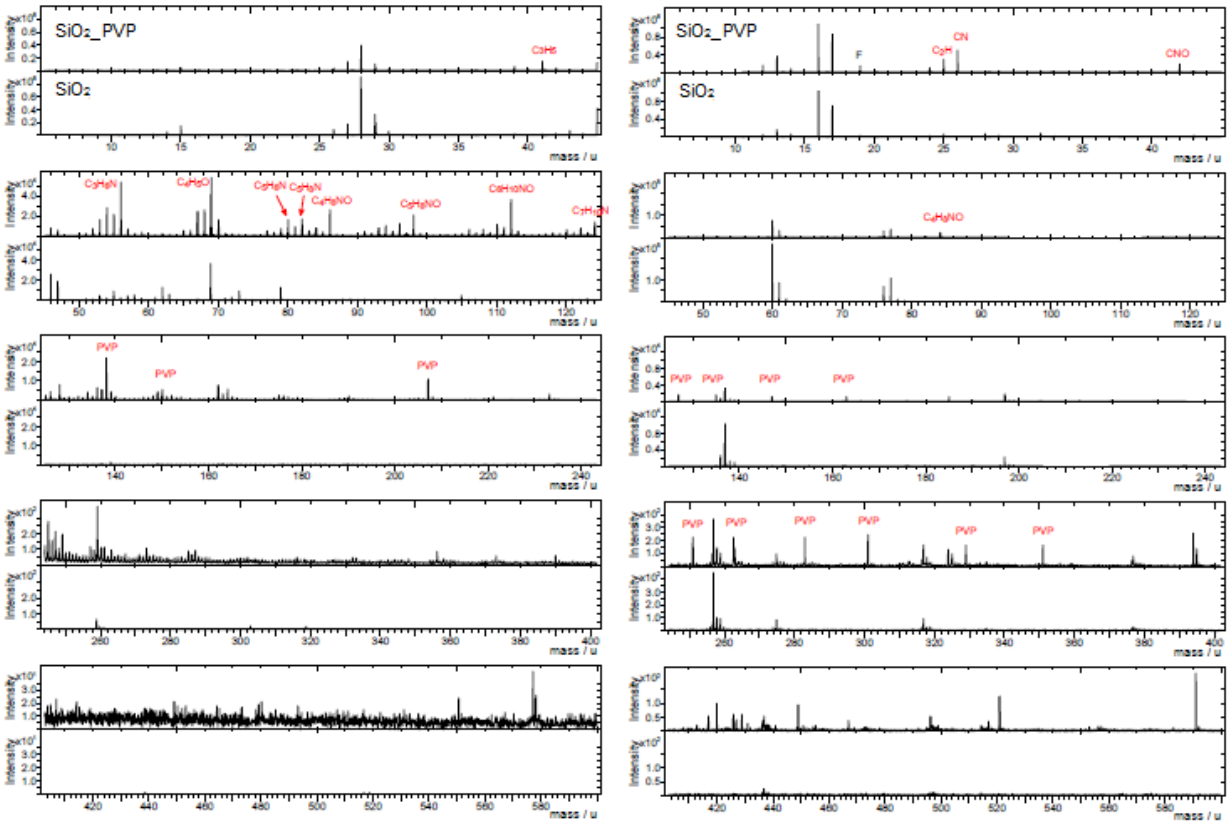

Figure S3-C. ToF-SIMS analysis for (c) SiO_2_ PVP in comparison to not functionalized SiO_2 NPs obtained from positive (left) and negative (right) polarity.

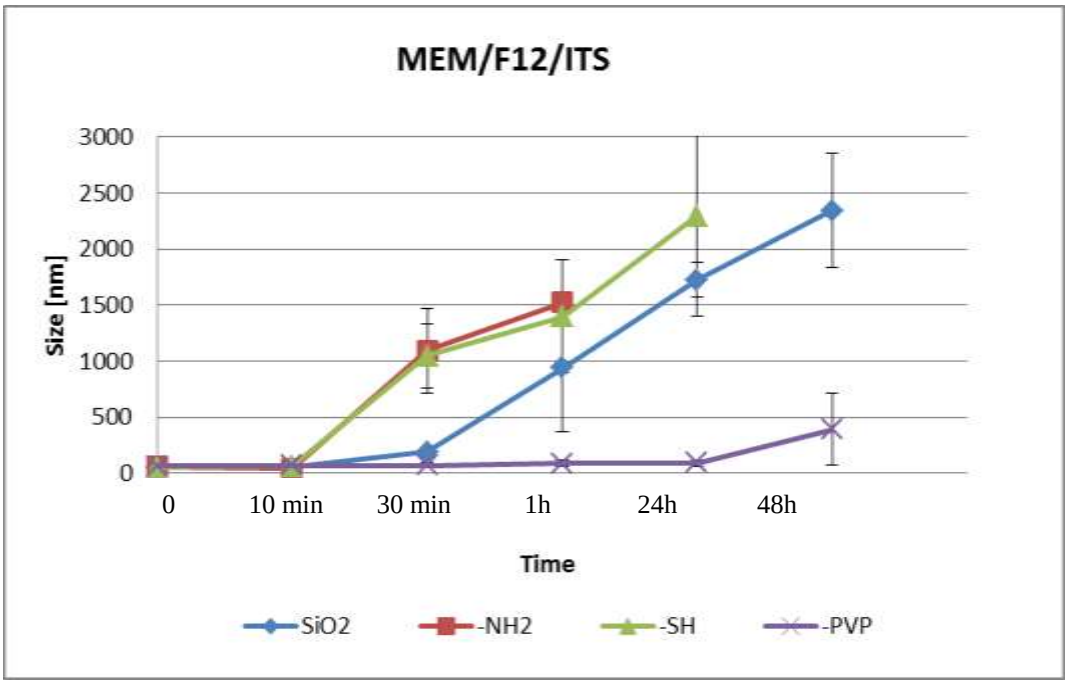

Figure S4. Time and functionalization depended SiO_2 NPs stability in MEM/F12/ITS medium analyzed with DLS: number distribution.

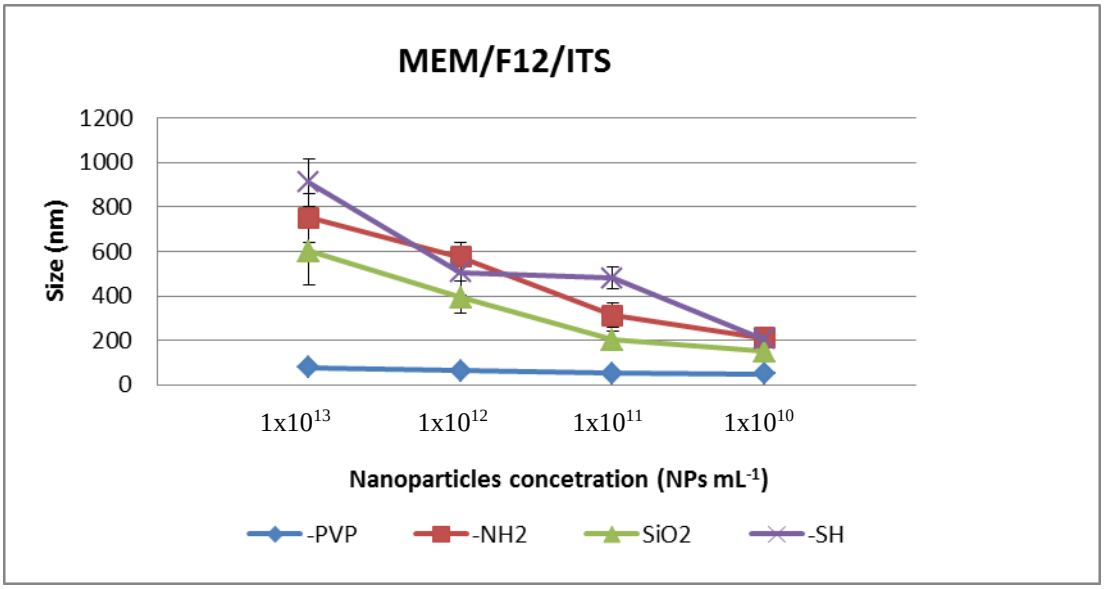

Figure S5. Concentration and functionalization depended SiO_2 NPs stability in MEM-F12-ITS medium analyzed with DLS: number distribution.

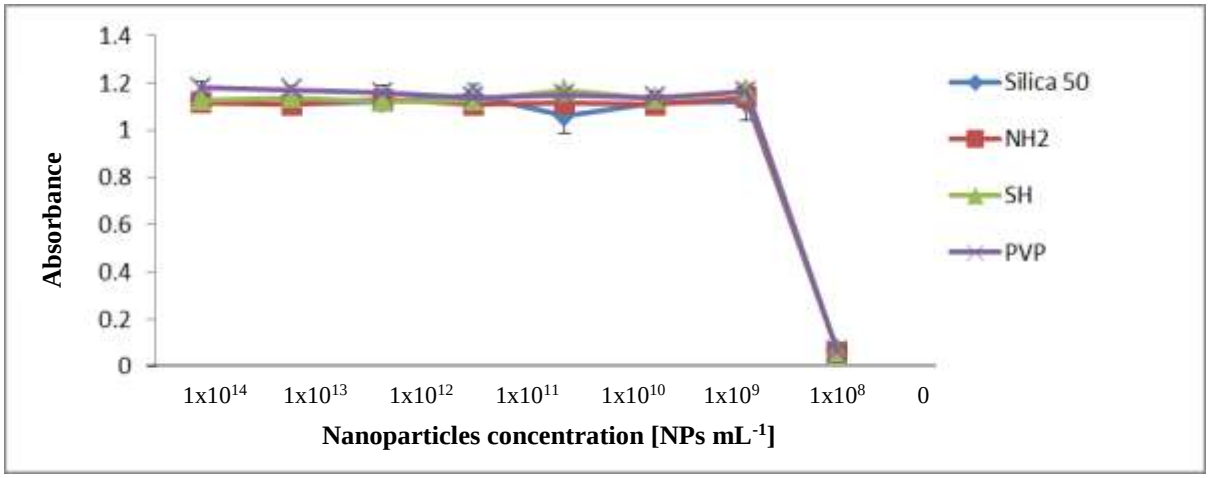

Figure S6. Interference of differently functionalized SiO_2 NPs with LDH assay. NPs were incubated in MEM-F12-ITS medium containing 2 U mL^{-1} of LDH enzyme for 48 h at 37 °C in a CO_2 incubator.

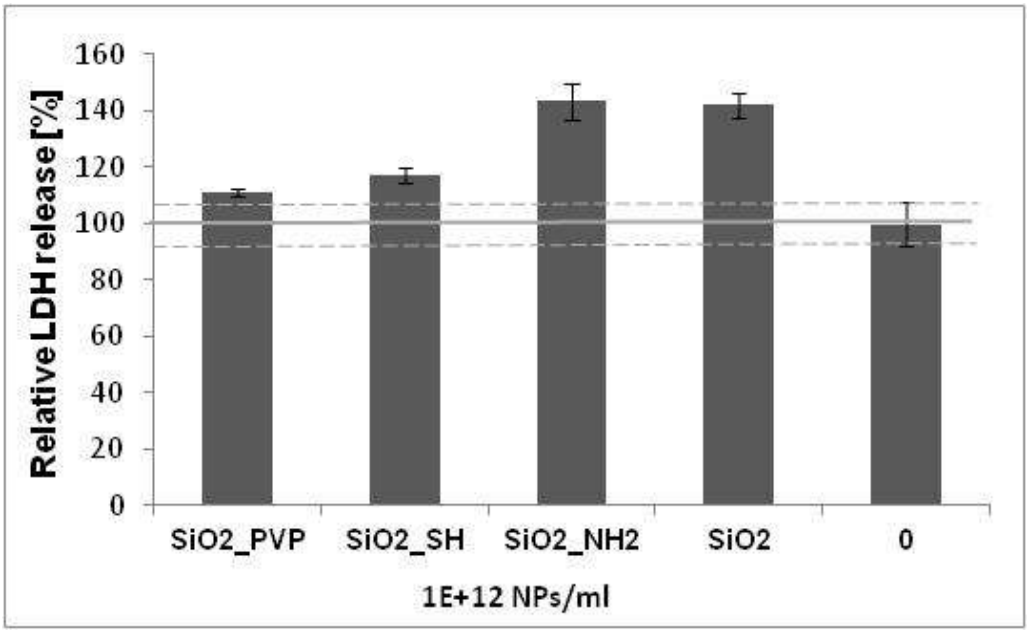

Figure S7. LDH assay for microglia cells; 0: non-treated cells.

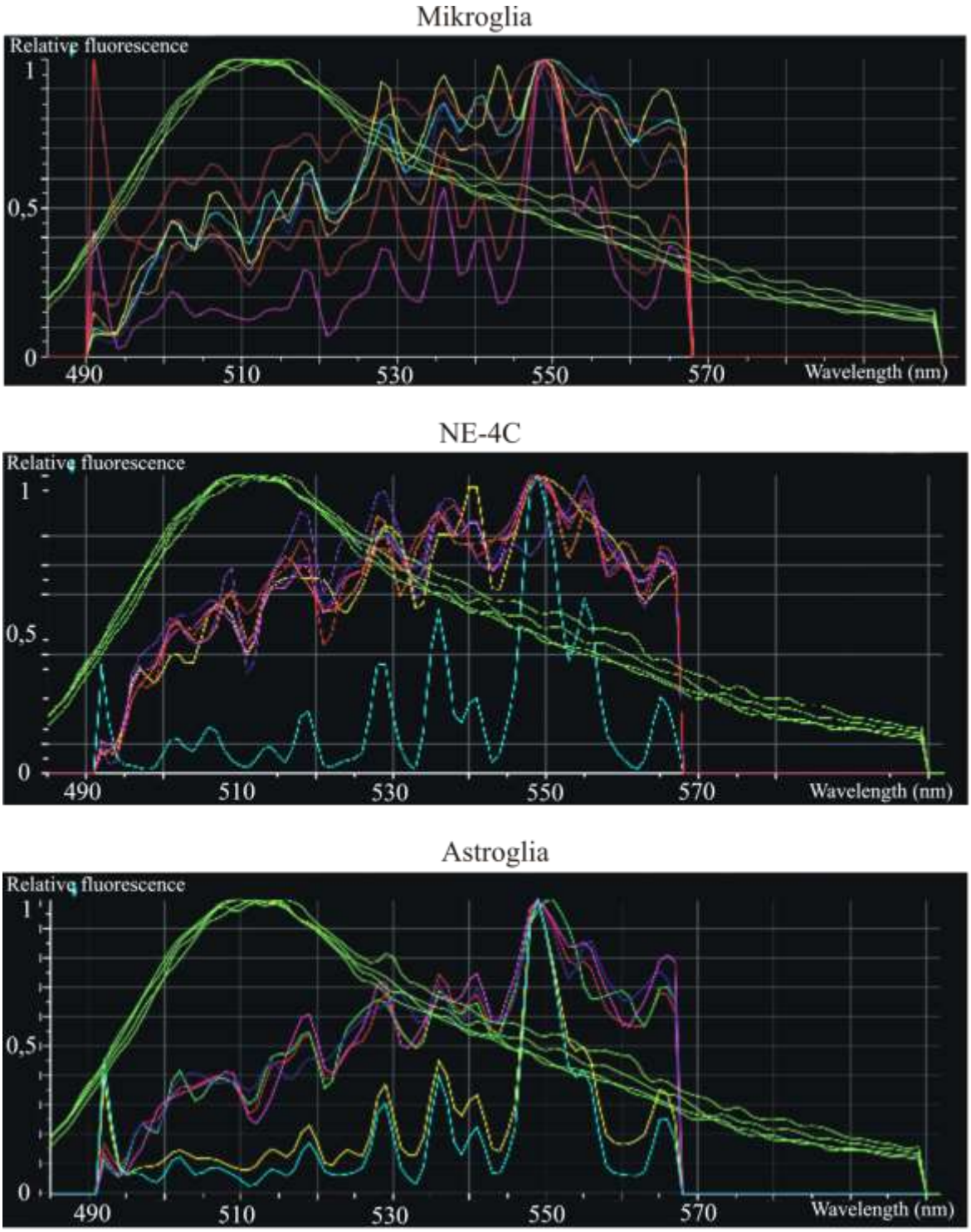

Figure S8. Fluorescence of SiO_2, SiO_2_NH_2, SiO_2_SH NPs as positive control (green); autofluorescence of microglia, NE-4C and astroglia cells as negative controls (other colors).